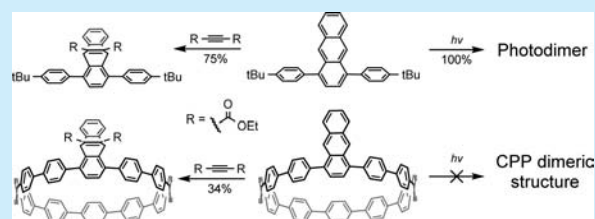


## Investigating the Reactivity of 1,4-Anthracene-Incorporated Cycloparaphenylene

Penghao Li,<sup>†</sup> Bryan M. Wong,<sup>‡</sup> Lev N. Zakharov,<sup>§</sup> and Ramesh Jasti<sup>\*,†</sup><sup>†</sup>Department of Chemistry & Biochemistry, University of Oregon, Eugene, Oregon 97403, United States<sup>‡</sup>Department of Chemical & Environmental Engineering and Materials Science & Engineering Program, University of California, Riverside, California 92521, United States<sup>§</sup>CAMCOR, University of Oregon, 1443 East 13th Avenue, Eugene, Oregon 97403, United States

## Supporting Information

**ABSTRACT:** Cycloparaphenylenes (CPPs) and their derivatives are unique conjugated macrocycles with novel optoelectronic and host–guest properties. A better understanding of their reactivity is essential for creating new functional materials utilizing these strained aromatic molecules as building blocks. 1,4-Anthracene-incorporated CPP **1** was synthesized and exhibited Diels–Alder reactivity but was unable to photodimerize. Comparison studies with cyclophane **2** and unstrained **3** indicated that the distorted anthracene geometry is likely the major contributor to the anomalous reactivity of **1**.



The development of novel synthetic porous materials has a direct impact on a variety of technologies such as catalysis, separation, gas storage, and electronics.<sup>1</sup> These porous materials are commonly prepared by linking organic building units through covalent bonds (covalent organic frameworks and porous polymers),<sup>2</sup> metal coordination (metal organic frameworks),<sup>3</sup> or noncovalent interactions (porous molecular solids).<sup>4</sup> In addition to the collective effects of the entire building components, porous materials also inherit the intrinsic properties of their organic building blocks.<sup>1</sup> Therefore, developing novel molecular building blocks with unique properties is beneficial in expanding the applications of porous materials.

Cycloparaphenylenes (CPPs) are conjugated molecules with hoop-shaped backbones comprised of 1,4-connected benzene rings.<sup>5</sup> These strained aromatics and their related macrocyclic structures have potential materials applications owing to their ring-size dependent optoelectronic properties,<sup>6</sup> selective host–guest properties,<sup>5f,7</sup> as well as scalable gram-scale syntheses.<sup>5f,j,1</sup> We have been interested in utilizing CPPs as building blocks to construct new carbon materials, which would potentially preserve the useful properties of CPPs including discrete porosity and tunable electronic behavior.<sup>5k</sup> Herein, we report the synthesis, characterization, and reactivity study of 1,4-anthracene-incorporated [12]CPP **1** (Figure 1), in order to evaluate the practicality of utilizing anthracene as the reactive functional handle for cross-linking CPP-related molecules. Additionally, compounds **2** and **3** were prepared and studied to further elucidate the structural influence on the reactivity of the 1,4-diphenylanthracene (DPA) core.

The versatility and adaptability of anthracene chemistry have enabled chemists to create sophisticated architectures from complex molecules<sup>8</sup> to functional polymeric materials.<sup>9</sup> Recently, two-dimensional polymers (2DPs) were successfully prepared

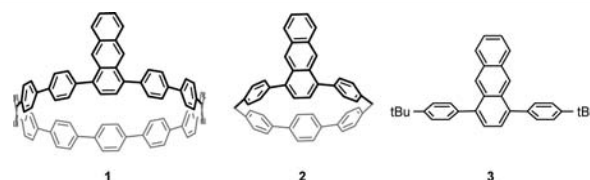


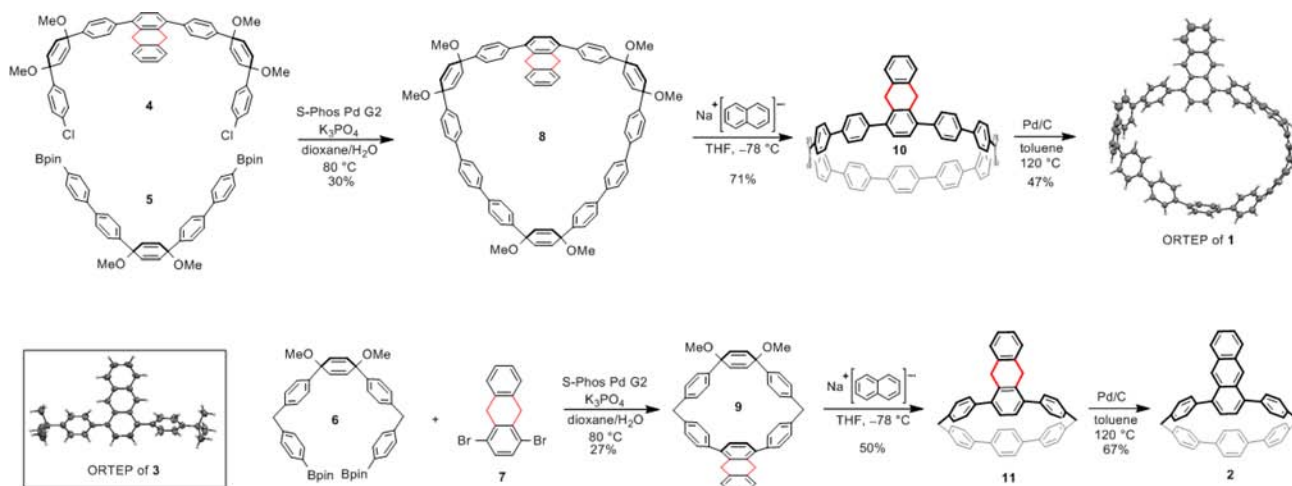
Figure 1. Structures of 1–3.

from the cycloaddition reactions of anthracene-containing monomers.<sup>10</sup> We envisioned that CPP structures with multiple 1,4-anthracene subunits could potentially be cross-linked to produce new types of network structures in a similar fashion as the case of 2DPs. However, previous seminal works on anthracenophanes suggest that the strained anthracene unit of **1** might have different reactivity compared to the planar counterparts.<sup>11</sup> Moreover, the substituent effect from the neighboring bent oligophenylene fragment might also impact the reactivity of the anthracene in **1**. Thus, we designed a strained cyclophane structure **2** that is free from the influence of this substituent effect, as well as a planar 1,4-DPA molecule **3**, in order to determine the key factors (bent geometry or substituent effect) that governs the reactivity of **1**. In this paper, we surveyed the reactivity of **1–3** in photoinduced [4 + 4]-cycloaddition reactions and thermal Diels–Alder (DA) reactions, in combination with theoretical analyses to rationalize the structure–reactivity relationships.

In planning the synthesis of macrocyclic structures **1** and **2**, we adapted the generic strategy of CPP chemistry,<sup>6b</sup> which takes advantage of the curved cyclohexadiene building units to

Received: February 14, 2016

Published: March 22, 2016

Scheme 1. Synthesis of **1** and **2** from 9,10-Dihydroanthryl Intermediates; X-ray Single Crystal Structures of **1** and **3** (ORTEP)

assemble a less strained macrocyclic precursor which can be later aromatized to produce the target molecular skeleton. However, our initial synthetic attempt using anthryl intermediates failed to deliver isolable final products **1** and **2** (Scheme S1). We discovered that compounds **1** and **2** are unstable in the presence of light and oxygen, presumably due to the formation of labile endoperoxides.<sup>11a,12</sup> Inspired by Miller's works on hydrogen-protected acenes,<sup>13</sup> we developed a two-step aromatization strategy employing intermediates with a 9,10-dihydroanthryl moiety, which allowed for the purification and subsequent characterization of **1** and **2** in a glovebox with a chemically inert N<sub>2</sub> atmosphere. Depicted in Scheme 1, the synthesis of macrocycles **8** and **9** was achieved by applying a Suzuki coupling condition using a S-Phos Gen II precatalyst<sup>14</sup> from corresponding coupling partners in 30% and 27% yield, respectively. Treating **8** and **9** with single electron reductant sodium naphthalenide at  $-78\text{ }^{\circ}\text{C}$  followed by quenching the reaction with I<sub>2</sub> gave the corresponding dihydroanthryl precursors **10** (71%) and **11** (50%). Finally, heating **10** or **11** with Pd/C in degassed toluene successfully yielded respective target molecule **1** (47%) or **2** (67%). Additionally, compound **3** and key intermediates **4**–**7** were easily prepared, and the synthetic details are provided in the Supporting Information (SI). The structures of **1**–**3** were confirmed by NMR (<sup>1</sup>H, <sup>13</sup>C), IR, and mass spectrometry (SI).

With these compounds in hand, we first investigated their electronic structures utilizing cyclic voltammetry and theoretical calculations. The first oxidation peaks for **1**–**3** are reversible with respective half wave potentials at 0.65, 0.60, and 0.72 V (vs Fc/Fc<sup>+</sup>) (SI). As Density Functional Theory (DFT, B3LYP/6-31G\*)<sup>15</sup> calculations predicted that the highest occupied molecular orbital (HOMO) and the lowest unoccupied molecular orbital (LUMO) mainly delocalize on the DPA cores for compounds **1**–**3** (SI), we confirmed that the measured first oxidation potentials truly represent the HOMO energy levels of the DPA segments. This observation of higher-lying HOMO energy levels in **1** and **2** compared to **3** is consistent with our previous finding that bending destabilizes the HOMO of the polycyclic aromatic hydrocarbons (PAHs).<sup>16</sup> We also observed an increasing calculated HOMO/LUMO energy gap from **1** (3.06 eV) to **2** (3.22 eV) to **3** (3.42 eV).

Next, we characterized the photophysical properties of **1**–**3** (Figure 2). The UV–vis spectra of **1** exhibit an intense [12]CPP backbone absorption band ( $\lambda_{\text{max}} = 338\text{ nm}$ ),<sup>5a</sup> as well as

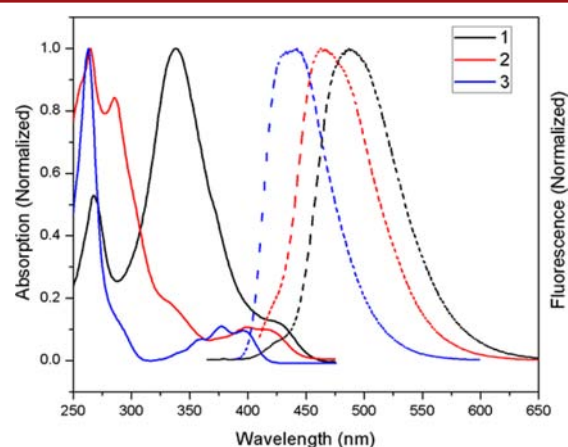
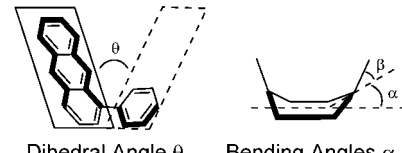


Figure 2. UV–vis absorption and fluorescence data of **1**–**3** (measured in DCM solutions).

anthracene absorption bands ( $\lambda_{\text{max}} = 268\text{ nm}$  and the broad band from 400 to 460 nm). Similarly, **2** displays both the *p*-terphenyl absorption ( $\lambda_{\text{max}} = 285\text{ nm}$ ) and the anthracene absorption ( $\lambda_{\text{max}} = 268\text{ nm}$  and the broad band from 370 to 450 nm). For **3**, the UV–vis spectra feature a characteristic anthracene absorption structure with well resolved vibrational bands ( $\lambda_{\text{max}} = 363\text{ nm}$ ) and a high energy band at 263 nm.<sup>17</sup> From the onset absorption data, we calculated the optical band gaps to be 2.72 eV (**1**), 2.78 eV (**2**), and 2.98 eV (**3**), which is consistent with the trend of theoretical HOMO/LUMO energy gaps (SI). Furthermore, TD-DFT calculations (B3LYP/6-31G\*)<sup>15</sup> predicted that the lowest energy absorptions of **1**–**3** can be assigned to the HOMO/LUMO transitions of the DPA cores (SI). The fluorescence spectra were also recorded, where the emissions exhibit a hypsochromic shift from **1** (487 nm), to **2** (463 nm), to **3** (442 nm).

We were able to obtain single crystals of **1** and **3** suitable for X-ray crystallography (Scheme 1 and Figures S9–S10). For comparison, DFT calculations (B3LYP/6-31G\*)<sup>15</sup> were also performed to optimize the molecular geometries. Notably, the calculated molecular structures of **1** and **3** are in good agreement with the empirical X-ray crystal structures (Table S1). By analyzing the calculated structural data (Table 1), we found that the DPA cores of **1** and **2** have similar deformation angles  $\alpha$  ( $7.4^{\circ}$ ,  $9.5^{\circ}$ ), bent angles  $\beta$  ( $6.7^{\circ}$ ,  $8.9^{\circ}$ ), and torsional angles  $\theta$  ( $42.8^{\circ}$ ,

**Table 1.** Calculated Structural Properties of 1–3 (DFT, B3LYP/6-31\*)


entry	$\theta$ , deg <sup>a</sup>	$\alpha$ , deg	$\beta$ , deg
1	42.8	7.4	6.7
2	43.0	9.5	8.9
3	54.5	4.5	0.7

<sup>a</sup>Dihedral angles shown are average values.

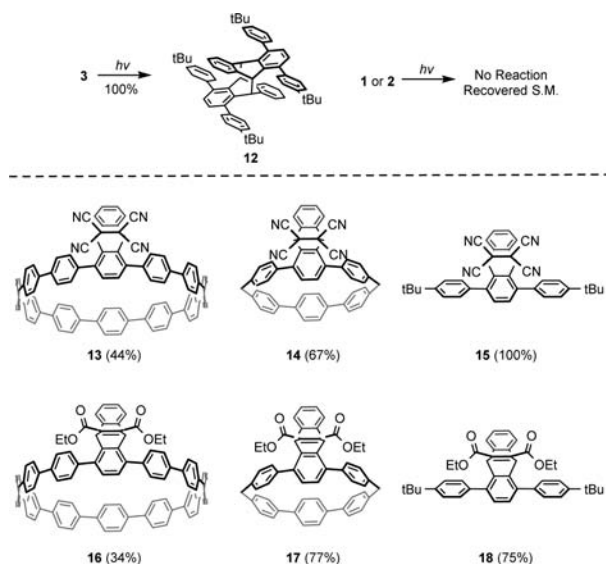
43.0°). By comparing **2** to **3**, it can be seen that the ring strain causes a decrease in torsional angles and an increase in the bent and deformation angles, which agrees with the observed trend when comparing CPPs to linear oligoparaphenylenes (LPPs).<sup>6a,18</sup> Additionally, the calculated strain energies<sup>19</sup> on the DPA cores of 1–3 were 56.34, 62.04, and 4.78 kcal/mol, respectively. Interestingly, the strain energy trend correlates well with the experimental trend of HOMO energy levels determined from the cyclic voltammetry. Overall, our electrochemical, photophysical, and theoretical studies demonstrated that the DPA cores in **1** and **2** share similar electronic and geometric characters that are distinct from those of **3**.

With this information in hand, we examined the photodimerization and DA reactions of these anthracene-containing compounds. Upon UV irradiation, **3** undergoes [4 + 4]-cycloaddition to generate the head-to-tail photodimer **12** in quantitative yield (Scheme 2). In contrast, no reactions were observed for **1** and **2** when similar conditions were applied. Changing the light source to a different wavelength or altering solvent polarity still produced no photodimer products for **1** and **2**. We also attempted crossover experiments by mixing excess **3** with either **1** or **2** only to observe photodimer **12** and unreacted **1**

or **2**. As for DA reactions, 1–3 readily reacted with dienophiles tetracyanoethylene (TCNE) and diethyl acetylenedicarboxylate to produce the corresponding DA-adducts **13**–**18**, of which the new bonds form at the 9,10-position of the anthracene core (Scheme 2). As **1** and **2** have higher-lying HOMO levels compared to **3**, it is expected that **1** and **2** should be more reactive with dienophiles than **3**.<sup>20</sup> Surprisingly, **1** and **2** show no DA reactivity with C<sub>60</sub> while the DA-adduct of **3** with C<sub>60</sub> was observed under similar and less energetic conditions (SI). Additionally, we synthesized 1,4-anthracene incorporated [10]CPP, which is also unreactive with C<sub>60</sub>, though the host–guest complex was observed as expected (SI). These reaction studies clearly indicated that compound **2** exhibits identical reactivity as **1**, from which we conclude that the distorted anthracene geometry is likely the main contributor to the anomalous photochemical and DA reactivity of **1** compared to unstrained **3**.

In order to rationalize the relationship between the distorted anthracene geometry and the observed anomalous reactivity, we conducted theoretical calculations at the  $\omega$ B97XD/6-31G\*<sup>15,21</sup> level of theory to analyze the reaction free energies and the transition state energy barriers. Since our calculations omitted the configurational entropic factors ( $\Delta S$ ), the actual free energy ( $\Delta G = \Delta H - T\Delta S$ ) is higher than the calculated values ( $T\Delta S > 0$ ).<sup>22</sup> We found that the reaction free energy for dimerization of **1** is endergonic (1.2 kcal/mol), which alone indicates that the dimerization is not favored in terms of thermodynamics. The free energies for the dimerization of **2** and **3** are exergonic with respective values of –1.6 and –6.7 kcal/mol. It is possible the change of the entropy for the dimerization of **2** is pronounced enough that the reversed dissociation reaction is favored.<sup>23</sup> We also calculated the reaction barriers for each of the cases but found that the transition state structures exhibited broken-symmetry and multireference effects which are beyond the scope of the single-reference DFT approach used here.<sup>24</sup> Additionally, the reaction free energies for DA reactions of C<sub>60</sub> with 1–3 are all calculated to be exergonic (**1**, –16.0 kcal/mol; **2**, –15.6 kcal/mol; **3**, –20.9 kcal/mol) and the activation free energies for 1–3 are determined to be 17.9, 16.9, and 12.7 kcal/mol, respectively. Though no definitive conclusion could be made regarding the reaction outcomes from these data, the DA reaction of C<sub>60</sub> with **3** is suggested to be both kinetically and thermodynamically favored. Likewise, the configurational entropy (i.e., the number of possible molecular configurations increases in the order of **3**, **2**, and **1**) could play an important role in differentiating the DA reaction outcome between **1** (**2**) and **3**. Thus, our theoretical analysis seemed to suggest that the bent geometry influences the reactivity by elevating the transition energy barriers and by destabilizing the products.

In conclusion, we have synthesized and characterized 1,4-anthracene incorporated [12]CPP **1** and two reference compounds **2** and **3**. We discovered that **1**, though unable to photodimerize, can still react with certain dienophiles. Therefore, the DA reaction is a potential strategy to construct new carbon materials from anthracene-incorporated CPPs. Additionally, through the comparison studies with reference compounds **2** and **3**, we determined that the unusual reactivity of **1** is likely to originate from the bent and distorted geometry, rather than the substituent effect from the backbone. Importantly, our work suggests that the change in the reactivity of strained PAHs should be taken into consideration when planning cross-linking strategies.

**Scheme 2.** Photodimerization of 1–3; DA-Adducts of 1–3 with Tetracyanoethylene (**13**–**15**) and with Diethyl Acetylenedicarboxylate (**16**–**18**)<sup>a</sup><sup>a</sup>Isolated yield (%) shown in parentheses.



## ■ ASSOCIATED CONTENT

## ■ Supporting Information

The Supporting Information is available free of charge on the ACS Publications website at DOI: [10.1021/acs.orglett.6b00430](https://doi.org/10.1021/acs.orglett.6b00430).

Detailed experimental procedures; NMR spectra; crystallographic, photochemical, and electrochemical data; computational details and coordinates (PDF)

## ■ AUTHOR INFORMATION

## Corresponding Author

\*E-mail: [rjasti@uoregon.edu](mailto:rjasti@uoregon.edu).

## Notes

The authors declare no competing financial interest.

## ■ ACKNOWLEDGMENTS

Financial support was provided by the National Science Foundation (CH-1255219), the Sloan Foundation, the Camille and Henry Dreyfus Foundation, and generous startup funds from the University of Oregon. B.M.W. acknowledges the National Science Foundation for the use of supercomputing resources through the Extreme Science and Engineering Discovery Environment (XSEDE), Project No. TG-CHE150040. The authors would like to gratefully acknowledge Jonathan L. Marshall (University of Oregon) for assistance with cyclic voltammetry.

## ■ REFERENCES

- (1) For a comprehensive review, see: Slater, A. G.; Cooper, A. I. *Science* **2015**, *348*, aaa8075.
- (2) (a) Feng, X.; Ding, X.; Jiang, D. *Chem. Soc. Rev.* **2012**, *41*, 6010. (b) Xu, Y.; Jin, S.; Xu, H.; Nagai, A.; Jiang, D. *Chem. Soc. Rev.* **2013**, *42*, 8012. (c) Ding, S.-Y.; Wang, W. *Chem. Soc. Rev.* **2013**, *42*, 548.
- (3) (a) Kreno, L. E.; Leong, K.; Farha, O. K.; Allendorf, M.; Van Duyne, R. P.; Hupp, J. T. *Chem. Rev.* **2012**, *112*, 1105. (b) Lee, J.; Farha, O. K.; Roberts, J.; Scheidt, K. A.; Nguyen, S. T.; Hupp, J. T. *Chem. Soc. Rev.* **2009**, *38*, 1450.
- (4) Zhang, G.; Mastalerz, M. *Chem. Soc. Rev.* **2014**, *43*, 1934.
- (5) (a) Jasti, R.; Bhattacharjee, J.; Neaton, J. B.; Bertozzi, C. R. *J. Am. Chem. Soc.* **2008**, *130*, 17646. (b) Sisto, T. J.; Golder, M. R.; Hirst, E. S.; Jasti, R. *J. Am. Chem. Soc.* **2011**, *133*, 15800. (c) Xia, J.; Golder, M. R.; Foster, M. E.; Wong, B. M.; Jasti, R. *J. Am. Chem. Soc.* **2012**, *134*, 19709. (d) Darzi, E. R.; Sisto, T. J.; Jasti, R. *J. Org. Chem.* **2012**, *77*, 6624. (e) Hirst, E. S.; Jasti, R. *J. Org. Chem.* **2012**, *77*, 10473. (f) Xia, J.; Bacon, J. W.; Jasti, R. *Chem. Sci.* **2012**, *3*, 3018. (g) Xia, J.; Jasti, R. *Angew. Chem., Int. Ed.* **2012**, *51*, 2474. (h) Hines, D. A.; Darzi, E. R.; Jasti, R.; Kamat, P. V. *J. Phys. Chem. A* **2014**, *118*, 1595. (i) Adamska, L.; Nayyar, I.; Chen, H.; Swan, A. K.; Oldani, N.; Fernandez-Alberti, S.; Golder, M. R.; Jasti, R.; Doorn, S. K.; Tretiak, S. *Nano Lett.* **2014**, *14*, 6539. (j) Evans, P. J.; Darzi, E. R.; Jasti, R. *Nat. Chem.* **2014**, *6*, 404. (k) Darzi, E. R.; Hirst, E. S.; Weber, C. D.; Zakharov, L. N.; Lonergan, M. C.; Jasti, R. *ACS Cent. Sci.* **2015**, *1*, 335. (l) Kayahara, E.; Patel, V. K.; Xia, J.; Jasti, R.; Yamago, S. *Synlett* **2015**, *26*, 1615. (m) Patel, V. K.; Kayahara, E.; Yamago, S. *Chem. - Eur. J.* **2015**, *21*, 5742. (n) Takaba, H.; Omachi, H.; Yamamoto, Y.; Bouffard, J.; Itami, K. *Angew. Chem., Int. Ed.* **2009**, *48*, 6112. (o) Omachi, H.; Matsuura, S.; Segawa, Y.; Itami, K. *Angew. Chem., Int. Ed.* **2010**, *49*, 10202. (p) Segawa, Y.; Miyamoto, S.; Omachi, H.; Matsuura, S.; Senel, P.; Sasamori, T.; Tokitoh, N.; Itami, K. *Angew. Chem., Int. Ed.* **2011**, *50*, 3244. (q) Ishii, Y.; Nakanishi, Y.; Omachi, H.; Matsuura, S.; Matsui, K.; Shinohara, H.; Segawa, Y.; Itami, K. *Chem. Sci.* **2012**, *3*, 2340. (r) Yamago, S.; Watanabe, Y.; Iwamoto, T. *Angew. Chem., Int. Ed.* **2010**, *49*, 757. (s) Iwamoto, T.; Watanabe, Y.; Sakamoto, Y.-I.; Suzuki, T.; Yamago, S. *J. Am. Chem. Soc.* **2011**, *133*, 8354. (t) Kayahara, E.; Sakamoto, Y.; Suzuki, T.; Yamago, S. *Org. Lett.* **2012**, *14*, 3284. (u) Kayahara, E.; Patel, V. K.; Yamago, S. *J. Am. Chem. Soc.* **2014**, *136*, 2284.
- (6) (a) Darzi, E. R.; Jasti, R. *Chem. Soc. Rev.* **2015**, *44*, 6401. (b) Golder, M. R.; Jasti, R. *Acc. Chem. Res.* **2015**, *48*, 557.
- (7) (a) Iwamoto, T.; Watanabe, Y.; Sadahiro, T.; Haino, T.; Yamago, S. *Angew. Chem., Int. Ed.* **2011**, *50*, 8342. (b) Iwamoto, T.; Watanabe, Y.; Takaya, H.; Haino, T.; Yasuda, N.; Yamago, S. *Chem. - Eur. J.* **2013**, *19*, 14061. (c) Iwamoto, T.; Slanina, Z.; Mizorogi, N.; Guo, J.; Akasaka, T.; Nagase, S.; Takaya, H.; Yasuda, N.; Kato, T.; Yamago, S. *Chem. - Eur. J.* **2014**, *20*, 14403. (d) Ueno, H.; Nishihara, T.; Segawa, Y.; Itami, K. *Angew. Chem., Int. Ed.* **2015**, *54*, 3707.
- (8) Yoshizawa, M.; Klosterman, J. K. *Chem. Soc. Rev.* **2014**, *43*, 1885.
- (9) Tasdelen, M. A. *Polym. Chem.* **2011**, *2*, 2133.
- (10) (a) Li, M.; Schlüter, A. D.; Sakamoto, J. *J. Am. Chem. Soc.* **2012**, *134*, 11721. (b) Kissel, P.; Erni, R.; Schweizer, W. B.; Rossell, M. D.; King, B. T.; Bauer, T.; Götzinger, S.; Schlüter, A. D.; Sakamoto, J. *Nat. Chem.* **2012**, *4*, 287. (c) Bhola, R.; Payamyar, P.; Murray, D. J.; Kumar, B.; Teator, A. J.; Schmidt, M. U.; Hammer, S. M.; Saha, A.; Sakamoto, J.; Schlüter, A. D.; King, B. T. *J. Am. Chem. Soc.* **2013**, *135*, 14134. (d) Kory, M. J.; Worle, M.; Weber, T.; Payamyar, P.; van de Poll, S. W.; Dshemuchadse, J.; Trapp, N.; Schlüter, A. D. *Nat. Chem.* **2014**, *6*, 779. (e) Murray, D. J.; Patterson, D. D.; Payamyar, P.; Bhola, R.; Song, W.; Lackinger, M.; Schlüter, A. D.; King, B. T. *J. Am. Chem. Soc.* **2015**, *137*, 3450.
- (11) (a) Tobe, Y.; Takahashi, T.; Ishikawa, T.; Yoshimura, M.; Suwa, M.; Kobi, K.; Kakiuchi, K.; Gleiter, R. *J. Am. Chem. Soc.* **1990**, *112*, 8889. (b) Tobe, Y.; Takahashi, T.; Kobi, K.; Kakiuchi, K. *J. Am. Chem. Soc.* **1991**, *113*, 5804. (c) Tobe, Y.; Takemura, A.; Jimbo, M.; Takahashi, T.; Kobi, K.; Kakiuchi, K. *J. Am. Chem. Soc.* **1992**, *114*, 3479.
- (12) Control experiments were conducted in which **1** or **2** was either exposed to light in a deoxygenated atmosphere or stored under air in a dark environment. Under either condition, **1** and **2** showed no evidence of decomposition. Thus we conclude that the decomposition of **1** and **2** is likely a photochemical process that requires both light and oxygen.
- (13) Athans, A. J.; Briggs, J. B.; Jia, W.; Miller, G. P. *J. Mater. Chem.* **2007**, *17*, 2636.
- (14) The ligand S-Phos is used to activate aryl chlorides for oxidative insertion in Suzuki–Miyaura coupling reaction. The structure of S-Phos Gen II precatalyst is provided in Scheme S5. For details about the Buchwald palladium precatalyst, see: Kinzel, T.; Zhang, Y.; Buchwald, S. L. *J. Am. Chem. Soc.* **2010**, *132*, 14073.
- (15) Selection of the level of theory for DFT calculations is described in the Supporting Information.
- (16) The bending effect here refers to both structural deformation and dihedral angle minimization. For details, see: Li, P.; Sisto, T. J.; Darzi, E. R.; Jasti, R. *Org. Lett.* **2014**, *16*, 182.
- (17) Becker, H. D. *Chem. Rev.* **1993**, *93*, 145.
- (18) Although strained, **1–2** are not as distorted as the anthracenophanes in ref 11.
- (19) The strain energies were calculated by subtracting the total energy of the optimized 1,4-diphenylanthracene from the total energies of DPA cores from **1–3** (terminated with hydrogen atoms). For details, see: Dobrowolski, M. A.; Cyrański, M. K.; Merner, B. L.; Bodwell, G. J.; Wu, J. I.; Schleyer, P. v. R. *J. Org. Chem.* **2008**, *73*, 8001.
- (20) Atherton, J. C. C.; Jones, S. *Tetrahedron* **2003**, *59*, 9039.
- (21) See the Supporting Information and: Chai, J. D.; Head-Gordon, M. *Phys. Chem. Chem. Phys.* **2008**, *10*, 6615.
- (22) Cao, Y.; Liang, Y.; Zhang, L.; Osuna, S.; Hoyt, A.-L. M.; Brisen, A. L.; Houk, K. N. *J. Am. Chem. Soc.* **2014**, *136*, 10743.
- (23) Jezowski, S. R.; Zhu, L.; Wang, Y.; Rice, A. P.; Scott, G. W.; Bardeen, C. J.; Chronister, E. L. *J. Am. Chem. Soc.* **2012**, *134*, 7459.
- (24) (a) Paldus, J.; Čížek, J. *Can. J. Chem.* **1985**, *63*, 1803. (b) Sherrill, C. D.; Lee, M. S.; Head-Gordon, M. *Chem. Phys. Lett.* **1999**, *302*, 425.